Geotechnical
Testing Journal

Kostas Senetakis[1] and Matthew Coop[2]

DOI: 10.1520/GTJ20120187

The Development of a New Micro-Mechanical Inter-Particle Loading Apparatus

VOL. 37 / NO. 6 / NOVEMBER 2014

Geotechnical Testing Journal

doi:10.1520/GTJ20120187 / Vol. 37 / No. 6 / November 2014 / available online at www.astm.org

Kostas Senetakis[1] and Matthew Coop[2]

The Development of a New Micro-Mechanical Inter-Particle Loading Apparatus

Reference

Senetakis, Kostas and Coop, Matthew, "The Development of a New Micro-Mechanical Inter-Particle Loading Apparatus," *Geotechnical Testing Journal*, Vol. 37, No. 6, 2014, pp. 1028–1039, doi:10.1520/GTJ20120187. ISSN 0149-6115

Manuscript received October 13, 2012; accepted for publication August 22, 2014; published online October 13, 2014.

[1] PhD, Lecturer, School of Civil and Environmental Engineering, University of New South Wales, Sydney, Australia (Corresponding author), e-mail: k.senetakis@unsw.edu.au

[2] PhD, Chair Professor, Dept. of Civil and Architectural Engineering, City Univ. of Hong Kong, Hong Kong, e-mail: mrcoop@cityu.edu.hk

ABSTRACT

The inter-particle coefficient of friction comprises an essential input parameter in computer codes that utilize the discrete element method. This paper describes the main features of a custom-built apparatus of a new generation, capable of performing inter-particle shearing tests at very small displacements on the order of tens to hundreds of microns and measuring the frictional forces developed at the contacts of coarse-grained particles of sand to gravel size. Linear, micro-stepping motors are used for the inter-particle shearing tests of a displacement-controlled type and the application of the vertical confinement of a force-controlled type at the particle contacts. The apparatus is designed to work at very small confining forces, in general between 1 and 20 N, and utilizes a system of bearings of small friction, which can be calibrated following simple procedures. The experiments are controlled and monitored through a computer code developed for the apparatus. The signal conditioning and data-logging systems were optimized to give the minimum environmental and electrical noise in the experimental data. The particles tested must have a relatively convex shape and be fairly symmetrical about the axis of shearing to avoid significant lateral forces in the out-of-plane horizontal direction during sliding, and, in general, the size of particles is limited from about 0.50 to 5.0 mm. Tests on reference particles composed of chrome steel balls and quartz particles demonstrated high repeatability of the results and agreement with the literature data. The experimentally derived horizontal force–displacement data showed that the stiffness of the apparatus is sufficiently high to prevent significant stick-slip phenomena, allowing a stable sliding.

Keywords

experimental micro-mechanics, inter-particle coefficient of friction, nonconforming surfaces, linear stepping-motor, bearing balls, linear bearing, stick-slip, stiffness, calibration, quartz particles

Introduction

The development of the discrete element method (DEM) (Cundall and Strack 1979; Cundall 1988) provided a valuable numerical tool that allowed the geotechnical research community to obtain insight into the micro-mechanical behavior of soils. Using DEM, complex phenomena and mechanisms that dominate particulate media have been studied, for example, the role of particle breakage and energy dissipation mechanisms in soils (e.g., Kuhn 1999; Lu and McDowell 2010; Shamy and Denissen 2011; Wang and Yan 2012, 2013), the role of the fabric on the engineering behavior of granular soils (e.g., Yimsiri and Soga 2011), creep phenomena in particulate media (e.g., Kuhn and Mitchell 1991; Kwok and Bolton 2010, as well as the response of soils at small strains (e.g., Yimsiri and Soga 2000). In past and recent studies, the important role of the inter-particle coefficient of friction on the monotonic and cyclic response of granular assemblies was also highlighted through DEM studies (e.g., Thornton and Sun 1993; Thornton 2000; Kruyt and Rothenburg 2006; O'Sullivan et al. 2008; Sazzad and Suzuki 2011; Barreto and O'Sullivan 2012; Wang and Yan 2013).

The interaction of particles in DEM is simulated using appropriate normal force–displacement and tangential force–displacement models (e.g., Thornton and Yin 1991; Vu-Quoc and Zhang 1999). Commonly, the normal stiffness is simulated based on the Hertz theory, while the Mindlin–Deresiewicz theory (Mindlin and Deresiewicz 1953), presented in Johnson (1985), is adopted for the tangential stiffness.

The tangential force–displacement relationships adopted in DEM are given as a function of the inter-particle coefficient of friction, and despite the increasing use of the DEM and the development of improved tangential force–displacement models (e.g., Vu-Quoc and Zhang 1999), the available experimental data relative to the inter-particle coefficient of friction at the contacts of coarse-grained particles and the frictional force–displacement relationships directly derived from laboratory investigations are fairly limited. Most experimental efforts in the past focused on shearing tests where a set of particles slide on the surface of a block of the same material, as, for example, in the experimental investigation by Horn and Deere (1962), or a block of different material, as, for example, in the study by Burwell and Rabinowicz (1953), which are easier to be implemented in the laboratory than sliding one particle against the surface of a second one, as, for example, in Skinner (1969), Barton (1972), and Cavarretta et al. (2010, 2011). However, in real soils and during sliding of a particle against the surface of another, there is the continuous development of new contacts, which may be not adequately represented by a block–block or particle to block types of contact. The other key difficulty with particle-to-block or block-to-block arrangements is that the flat surfaces of the blocks should have the same surface properties as the natural particles, which is not easily ensured. Using a contact between two natural particles avoids any such problem.

This paper presents the main features of a new, custom-built apparatus developed at City University of Hong Kong, capable of imposing and measuring forces and deflections at the contacts of coarse-grained particles in both the normal and tangential directions. The use of high-quality forces and displacement transducers, linear micro-stepping motors, signal conditioning, and data-logging systems allows accurate measurements in the range of very small displacements on the order of tens to hundreds of microns with a resolution of the forces and the displacements of about 0.02 N and 1 to 2 μm, respectively. The experiments are controlled and monitored through a new software developed for the apparatus.

The General Features and Basic Principles of the New Micro-Mechanical Apparatus

The basic principles of the design of the new apparatus are similar to the ones presented by Cavarretta et al. (2010, 2011). One particle of sand to gravel size is stationary in the direction of shearing, while a second one is imposed to slide against the surface of the former. Using simple geometry, the tangential and normal forces developed at the contact of the particles during the sliding are calculated based on the relative position of the particles, which is determined from the movement of the particles in the vertical direction. The horizontal force is applied through a linear micro-stepping motor and recorded by a load cell of low capacity and high resolution and stiffness. A key issue during the design of the apparatus was to allow the performance of inter-particle shearing tests at very small confining forces (i.e., 1 to 20 N), because recent studies using DEM (e.g., Barreto 2009) showed that the forces developed at the contacts of particles and for common engineering isotropic pressures are very small.

One difference between the new apparatus and that presented by Cavarretta et al. (2010, 2011) is that in the new one the lower particle is imposed to slide on the surface of the upper one, whereas, in Cavarretta et al. (2010, 2011), the lower particle was stationary. The most significant difference though is in the improvement of the stiffness of the system that allows the particles to be aligned close to their apexes at the start of the shearing without the occurrence of significant stick-slip that could lead to unstable sliding as described by Cavarretta et al. (2011). Stick-slip occurs when there is significant stored energy in an apparatus through its flexibility, manifesting itself by an increase of force followed by a sudden release, giving rise to an unstable or "saw-tooth" load-deflection behavior. Additionally, in the new apparatus, a second stepping motor is used through which the vertical confinement is applied at the contacts of the

FIG. 1

A general scheme of the inter-particle loading apparatus.

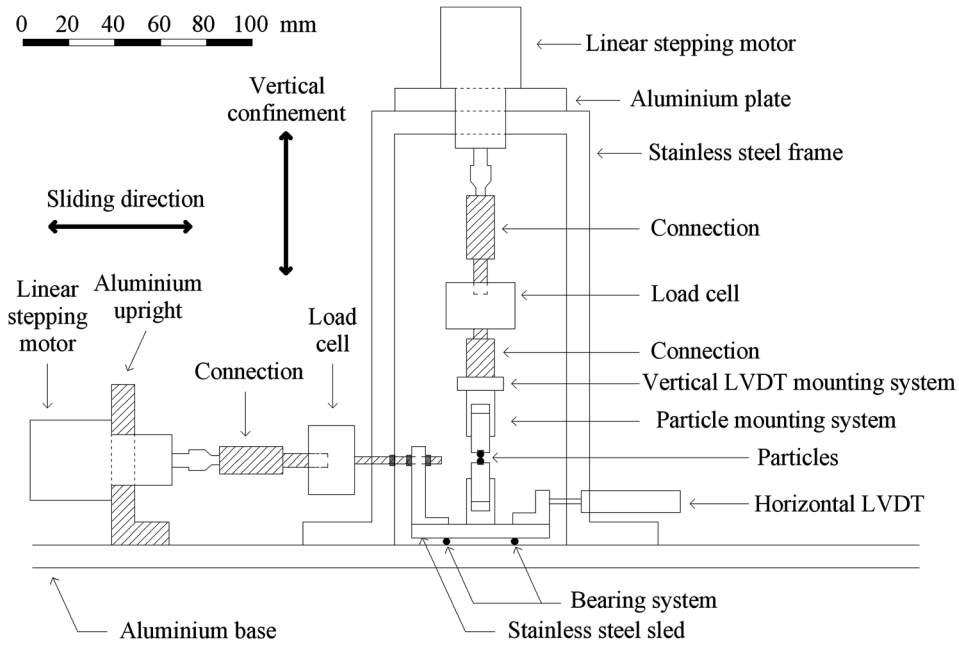

particles, whereas, in Cavarretta et al. (2010, 2011), dead loads were used for this purpose. The use of stepping motors gives improved control of forces and displacements applied to the particles during the test. Other key advantages of the new apparatus, compared to that of Cavarretta et al. (2011) are much simpler calibrations, data-correction methods, and experimental procedures, and also the direct measurement of the vertical load.

A general scheme of the new apparatus is given in **Fig. 1**. The lower particle is fixed on a stainless steel sled of 6.00 mm in thickness and 60 × 60 mm in plan. The sled and, thus, the lower particle is moved by a linear micro-stepping motor. A bearing system composed of three steel balls of 3.00 mm in diameter is used beneath the sled. Between the aluminum base of the apparatus and the sled, a thin layer of stainless steel is used that minimizes the friction produced by the bearing system. The motor, the load cell that records the horizontal force, and the mechanical parts that connect the stepping motor, the load cell, and the sled comprise the horizontal loading system of the apparatus. The upper stationary particle is fixed on the vertical loading system of the apparatus, which is composed of a vertical linear micro-stepping motor, a load cell that records the vertical force, and a series of connecting mechanical parts. The horizontal stepping motor, and thus the horizontal loading system is fixed on an aluminum upright that provides rigidity to the system in sliding, while the vertical stepping motor is attached to a stiff aluminum plate that is fixed on a stainless steel frame, which provides rigidity to the vertical loading system. Two different stainless steel frames, "frame 1" and "frame 2," of slightly different stiffnesses were used in this study.

One linearly variable differential transformer (LVDT) is used for the record of the movement of the sled in the direction of sliding, while one or two LVDTs are used for the record of the response of the upper particle in the vertical direction during the sliding of the lower one. A close-up view of the apparatus is given in **Fig. 2**. The armature of the vertical LVDT is connected to the sled through a linear bearing, which is commercially available. This bearing is composed of a block that is fixed on the sled and a rail that connects the armature of the LVDT to the horizontal loading system. The relative movement of the rail against the block is implemented through a system of small bearing balls. A close-up view of this bearing is given in **Fig. 3**.

FIG. 2 Close-up view of the apparatus: (1) particles in contact, (2) brass mount, (3) brass well, (4) armature of the vertical LVDT, (5) linear bearing, (6) body of the vertical LVDT, (7)–(8) mounting system of the vertical LVDT, and (9) mounting system of the horizontal LVDT.

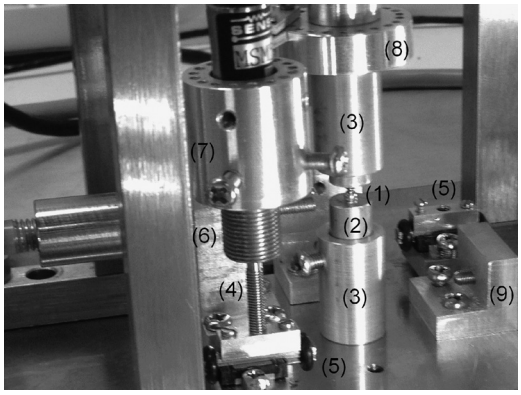

FIG. 3 Close-up view of the linear bearing: (1) block, (2) rail, (3) O ring, and (4) ball bearings.

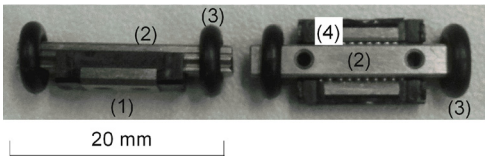

In the horizontal direction perpendicular to the direction of sliding, lateral confinement of the sled is provided through a fixed system of mechanical parts and bearings. However, it is noted that, although the force is measured along the direction of sliding and in the vertical direction, the horizontal forces along the perpendicular to the sliding direction cannot be measured with this system, so that it is important that the particles are relatively symmetrical in shape and are sheared over their apexes to avoid any significant out-of-plane forces. As shown in the schematic diagram of **Fig. 4**, the lateral confinement is implemented through a linear bearing. In particular, the block of the bearing is fixed on a small aluminum column, which is connected to the sled, and the rail of the bearing is connected through an M3 screw to an external column.

Two digital micro-cameras are used to check the out-of-plane alignment of the particles as well as for the recording of the inter-particle shearing tests in the direction of sliding. A typical alignment of particles (chrome steel balls) at the start of a shearing test is shown in **Fig. 5**. Because of the high stiffness of the horizontal loading system, the apparatus allows the initial positioning of the particles close to their apexes at the start of shearing without stick-slip occurring. **Figure 6** shows a general view of the apparatus using "frame 1," the digital micro-cameras, and a special designed cell, which is used for tests where the particles are immersed in a liquid.

FIG. 5 A typical alignment of particles (ball bearings) before the performance of an inter-particle shearing test.

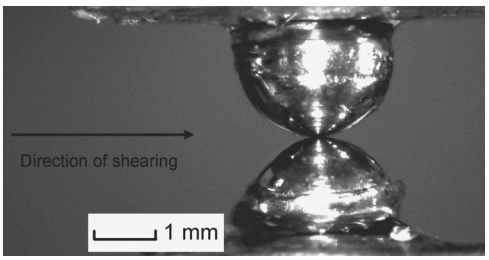

Mounting, Preparation and Alignment of Particles

The particles are fixed in cylindrical brass mounts of 17 mm in height and 8 mm in diameter (**Fig. 2**). The mounts have a small notch of diameter 0.80–0.85 and depth about 0.25–0.35 times the size of the particles to be tested. The particles are recessed in these notches using superglue. The mounts are placed on small brass wells and fixed using M3 screws. The upper well is attached to the vertical loading system while the lower one is attached on the stainless steel sled. To avoid contamination of the surfaces of the particles that might affect the experimental data (e.g., Barton 1972; Cavarretta et al. 2011), before the performance of the tests and after gluing the particles on the mounts, the surfaces of the particles are carefully cleaned using butanone.

Transducers, Micro-Stepping Motors, and Software

THE LINEAR MICRO-STEPPING MOTORS

The sliding of the lower particle against the surface of the upper stationary one and the vertical confinement at the contact of the

FIG. 4

A schematic diagram of the connection of the sled to the lateral (out-of-plan) confining system of the apparatus.

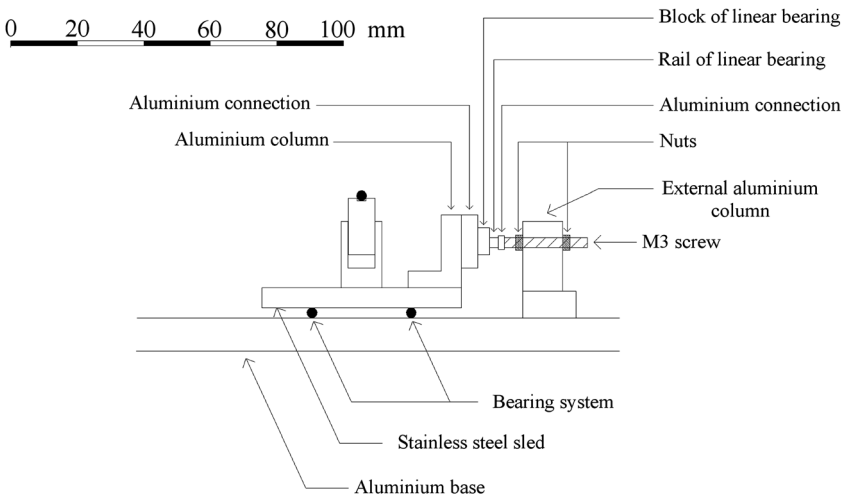

FIG. 6 Experiment on particles immersed in distilled water: (1) horizontal loading system in the direction of sliding, (2) stainless steel frame where the vertical loading system is attached, (3) aluminum base, (4) stainless steel thin layer beneath the bearing system of the sled, (5) cell for immersion the particles in liquid, and (6) digital micro-cameras for the alignment of the particles and recording of the tests.

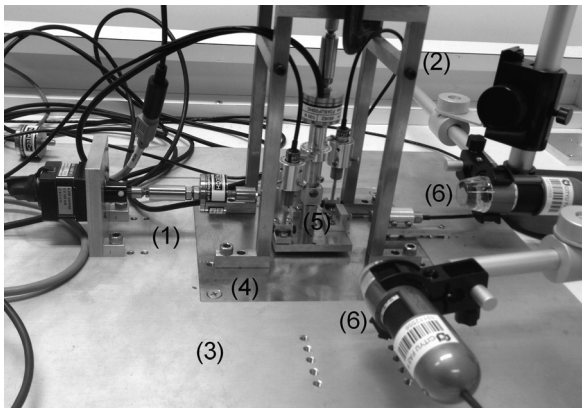

particles are implemented through linear micro-stepping motors. The main characteristics of these motors are summarized in **Table 1**. The high stiffness, the low backlash, and the repeatability are key factors for the choice of the stepping motors to be used. The minimum sliding velocity is 0.89 μm/s if the motors are controlled through the software provided by the manufacturer. However, a special control program written in QBASIC was developed to allow to the motors to be controlled with even lower velocities.

THE LOAD CELLS

Two load cells (type F245UF00H0, Novatech) of capacity equal to 100 N, stiffness of 3.2×10^6 N/mm, and repeatability of ± 0.02 N were used to record the horizontal and vertical forces at the contacts of the particles. Using high-quality amplifiers, signal conditioning, and data-logging systems, the overall effect of the environmental and the electrical noise on the data recorded by the load cells was minimized, providing results of high quality, adequate for micro-mechanical purposes. In **Fig. 7**, an example of the effect of the environmental and the electrical noise on the horizontal load cell is illustrated while there was no test in progress. In general, the effect of the noise produces a scatter less than ± 0.002 N on the data recorded by the load cells. The load cells were calibrated in both compression and tension using dead loads.

TABLE 1 The main characteristics of the linear micro-stepping motors (type NA14B16 linear actuator, NEMA size 14, and 16 mm travel, Zugo Photonics, Singapore).

Micro-step size	0.095 μm
Travel range	16 mm
Accuracy	+/− 30 μm
Repeatability	<5 μm
Backlash	<20 μm
Maximum speed	28 mm/s
Minimum speed[a]	0.00089 mm/s
Maximum continuous thrust	240 N
Linear motion per motor revolution	1.22 mm
Stiffness	400 N/mm

[a]The minimum speed may be lower because the stepping motors are controlled from a software developed for the apparatus.

THE LINEARLY VARIABLE DIFFERENTIAL TRANSFORMERS

The LVDTs, which record the horizontal and the vertical displacements during the shearing tests, are of a free armature type to avoid elastic energy being stored in the LVDTs during the tests, typically produced in spring return types. These LVDTs (type D6/02500U-L50, RDP) have a linear range of ± 2.5 mm with a resolution of less than ± 1 μm. As for the load cells, the LVDTs were calibrated against a micrometer in the laboratory following typical procedures. The effect of the environmental and electrical noise on the data recorded by the LVDTs was again minimized using high-quality amplifiers, signal conditioning, and data logging. Typical results that show the effect of the noise on the LVDTs while there was no test in progress are given in **Fig. 8**. In general, the effect of the noise produces a scatter of around ± 1 to ± 2 μm.

THE SOFTWARE AND THE OVERALL PERFORMANCE OF DISPLACEMENT- AND FORCE-CONTROLLED TESTS

The software developed for the apparatus allows both force- and displacement-controlled tests to be performed. Typically, the inter-particle shearing tests are of a displacement-controlled type, and the tests are performed with a target-sliding velocity provided by the stepping motor of the horizontal loading system. The vertical confinement is of a force-controlled type, and the stepping motor of the vertical loading system provides a target vertical force at the contact of the particles. In the software, there is a feedback between the stepping motors and the output from the load cells and/or the LVDTs. Inter-particle shearing

FIG. 7 The effect of the environmental and electrical noise on the data recorded by the load cells.

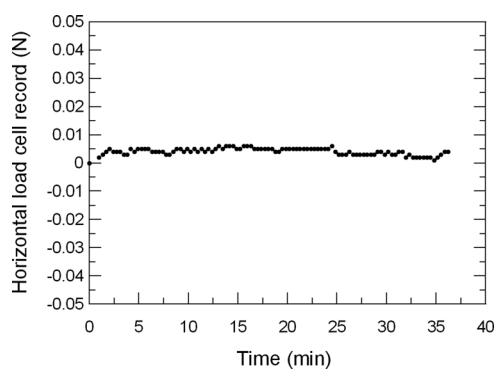

FIG. 8 The effect of the environmental and electrical noise on the data recorded by the LVDTs.

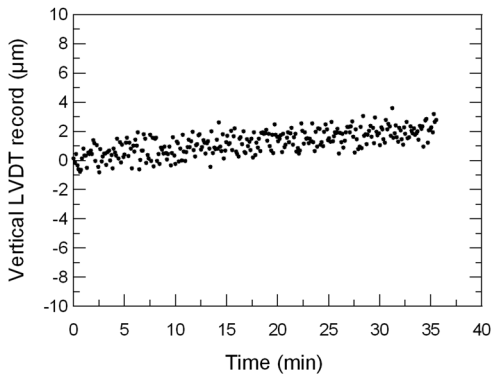

tests of a force-controlled type on quartz particles and comparisons with corresponding tests of a displacement-control type have been presented by Senetakis et al. (2013a), whereas comparisons on the stiffness and frictional characteristics at contacts of soil particles of variable types have been presented by Senetakis et al. (2013b). In this paper, the main focus is on the description of the equipment, the assessment of the repeatability of the shearing test results on reference particles, as well as the presentation of a limited number of test data on quartz particles to assess the possible convergence with literature data.

A typical example of the performance of the software in a displacement-controlled test is provided in **Fig. 9**, where the displacement measured by the horizontal LVDT (denoted as $\delta_{h,\text{measured}}$) is plotted against the target displacement used as input in the computer code (denoted as $\delta_{h,\text{target}}$). For a displacement-controlled test, the horizontal stepping motor moves a specific number of steps, which is a function of the target sliding velocity. There is then a short period of time for the data logging of the output from the horizontal LVDT, and then the stepping motor responds by moving the same or a different number of steps depending on the feedback from the horizontal LVDT.

FIG. 9 An example of the performance of the system computer code–stepping motor–horizontal LVDT during a typical displacement-controlled test in the direction of sliding.

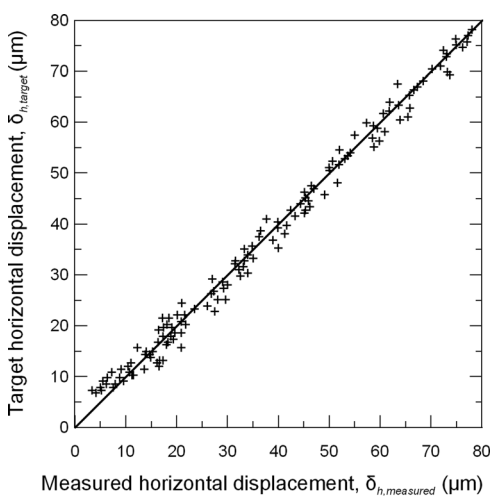

The Stiffness of the Apparatus in the Sliding and Vertical Directions

The stiffness of the apparatus in both the direction of sliding and the direction of the vertical confinement was evaluated experimentally. For this purpose, a "dummy sample" composed of a brass solid cylinder of the same diameter and twice the length of the brass mounts used in the inter-particle shearing tests was fixed between the lower and upper wells as shown in **Fig. 10**. This configuration approximates the system during a shearing test, but there are no particles attached to the brass mounts. By performing displacement- or force-controlled tests in the horizontal and vertical directions of this system, the stiffness of the apparatus in the horizontal and vertical directions could be determined.

STIFFNESS IN THE DIRECTION OF VERTICAL CONFINEMENT

The load cells are much stiffer than the stepping motors and thus the main sources of flexibility of the apparatus in the vertical direction are because of some deflection of the stepping motor and the bearing system beneath the sled. Typical results in terms of the vertical force against the vertical displacement during a displacement-controlled test using the "dummy sample" and "frame 1" are shown in **Fig. 11**. The system is extremely stiff in the vertical direction with a stiffness of about 1000 to 1500 N/mm. This stiffness is close to the stiffness of typical apparatuses used for particle-crushing tests, as, for example, the system described by Cavarretta et al. (2010). This high stiffness is attributed to the stainless steel frame to which the vertical loading system is attached.

FIG. 10 Typical configuration during the experimental evaluation of the stiffness of the apparatus: (1) "dummy sample," (2) lower well, and (3) upper well.

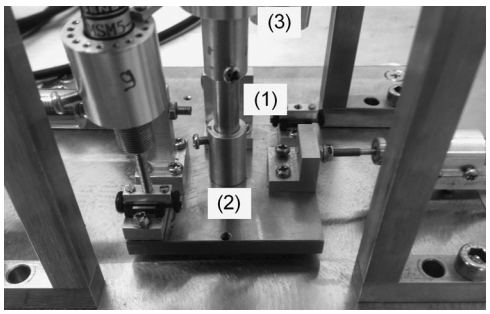

FIG. 11 The stiffness of the apparatus in the vertical direction.

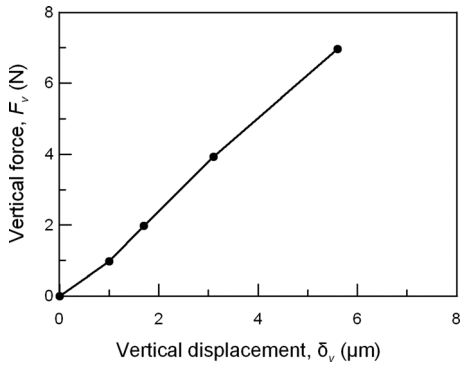

THE STIFFNESS OF THE APPARATUS IN THE DIRECTION OF SLIDING AND THE STIFFNESS OF THE SUPERGLUE USED TO FIX THE PARTICLES ON THE BRASS MOUNTS

In the direction of sliding, the main sources of flexibility of the system are because of some deflection of the stepping motor, the aluminum upright, the system that connects the stainless steel sled with the load cell, and some deflection of the vertical loading system and the frame in the direction of sliding. Typical results in terms of the horizontal force against the horizontal displacement during a displacement-controlled test using the "dummy sample" are shown in **Fig. 12(*a*)**. These results are for a vertical confining force of 5 N applied to the "dummy sample" by the vertical stepping motor.

In the horizontal direction, the stiffness of the system decreases with increasing displacement, with an initial value of 55 to 60 N/mm (when the "frame 1" or "frame 2" is used, respectively) at very small horizontal displacements to a value of 5 to 10 N/mm at about 200 μm of horizontal displacement. In contrast to the vertical system, the horizontal one is more flexible, but, as will be demonstrated later in this paper, the stiffness of the apparatus in the direction of sliding is sufficiently high to prevent stick-slip and allow a stable sliding when the particles are aligned close to their apexes at the start of the shearing tests. Even at large displacements of about 200 μm, the system shows a stiffness that is much higher in comparison to the stiffness at the contacts of non-conforming surfaces (i.e., not flat to flat) for which the stiffness decreases much more rapidly with increasing displacement.

Calibration tests were performed to evaluate the stiffness of the superglue that was used to fix the particles in the brass mounts. In these tests, two brass mounts were fixed to each other using a thin layer of superglue of a similar thickness of that used to fix the particles to the mounts. A typical shearing test of two brass mounts connected to each other with superglue is shown in **Fig. 12(*b*)**. This test is for a vertical confining force equal to 11 N. These calibration tests demonstrated that the stiffness of the system when the "dummy sample" is used (**Fig. 12(*a*)**) and when two brass mounts are glued together are very similar and, thus, the effect of the technique of fixing the particles on the mounts is expected to be fairly small on the experimental data.

FIG. 12 The stiffness of the apparatus in the direction of sliding (*a*) calibration test results using dummy sample (*b*) calibration test results where superglue is used to fix the brass mounts.

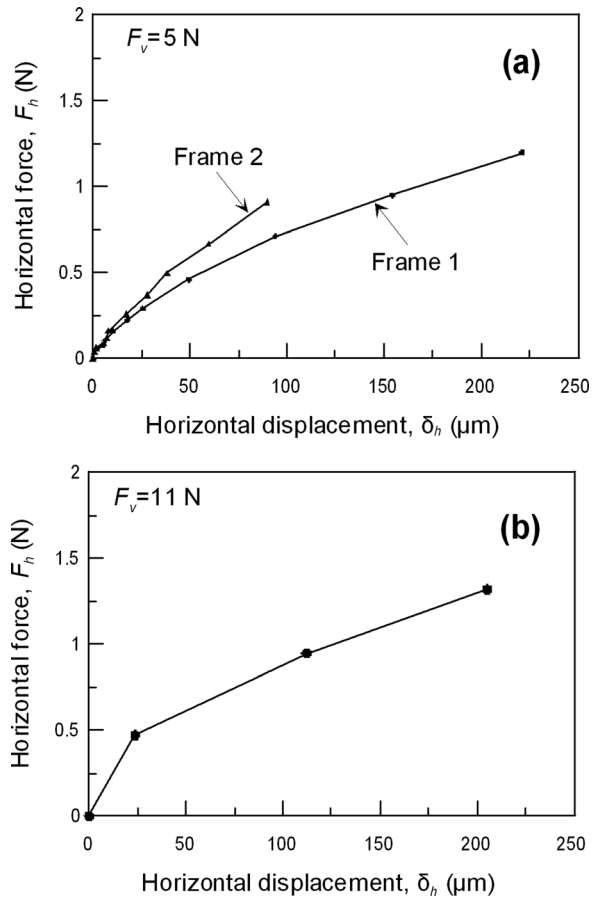

THE QUALITY OF THE EXPERIMENTAL DATA

The horizontal loading system should have sufficient stiffness to allow a stable sliding when the particles are aligned at initial positions close to their apexes without the occurrence of stick-slip. This was confirmed by inter-particle shearing tests on ball bearings (chrome steel balls) used as reference particles in this study. Typical test results on reference particles are shown in **Fig. 13**. In **Fig. 13(*a*)**, the horizontal force is plotted against the horizontal displacement, whereas, in **Fig. 13(*b*)**, the horizontal force is plotted against the time. The scatter of the data in **Fig. 13(*a*)** is partially the result of some relaxation at the contact of the particles, which might occur during the short periods of time that the stepping motor is stationary during pauses between control cycles. This small effect of relaxation at the contact of the particles on the experimental data is clearly shown in **Fig. 13(*b*)**. This possible relaxation interrupts the steady-state sliding leading to occurrence of stick-slip. However,

FIG. 13 Typical example of an inter-particle shearing test for reference particles (chrome steel balls of 2.37 mm in diameter).

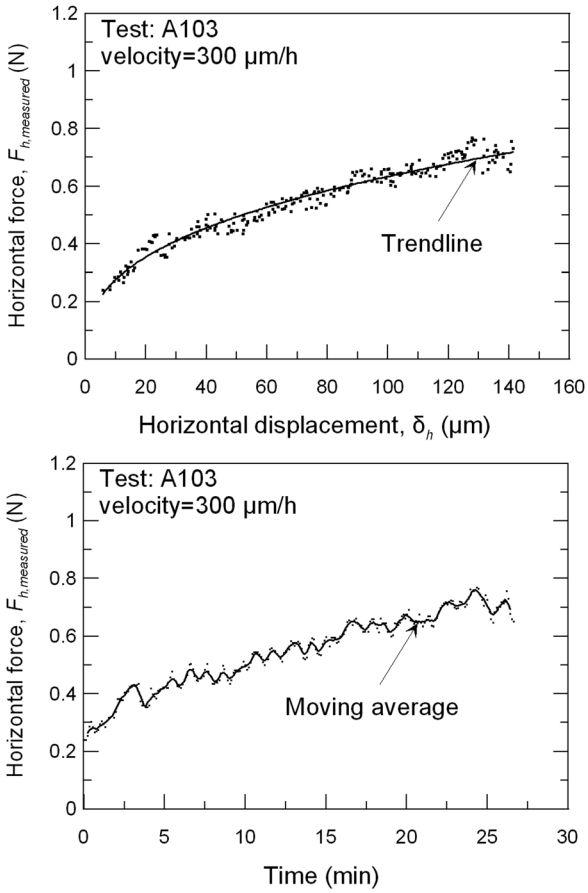

the overall quality of the experimental data is sufficient for the purpose of these tests and the stick-slip phenomena are not that significant, allowing a clear trend to be identified between the horizontal force and the horizontal displacement.

Correction of the Horizontal Force

The main sources of inherent friction of the apparatus during the inter-particle shearing tests are the following: (1) friction produced by the bearing system of the sled at zero external vertical load, (2) friction produced by the linear bearings used to fix the armature of the vertical LVDT to the sled and to connect the out-of-plan horizontal confining system to the sled, and (3) friction produced by the bearing system of the sled because of an external vertical load acting at the contact of the particles.

The friction produced by the first two sources, named $F_{h,b}$, was determined by performing calibration tests without external load while the sled is confined laterally by the out-of-plan system (**Fig. 4**) and the armature of the vertical LVDT is connected to the sled through the linear bearing (**Fig. 2**). The friction produced by the third source, named $F_{h,c}$, was determined by performing calibration tests at variable external vertical forces,

FIG. 14 Typical configuration during the calibration of the frictional force of the apparatus due to an external vertical load: (1) stepping motor, (2) stainless steel connection, (3) horizontal load cell, (4) aluminum connection, (5) aluminum upright, (6) stainless steel sled, (7) dead loads, (8) horizontal LVDT, (9) mounting system of horizontal LVDT, (10) stainless steel thin layer beneath the bearing system, and (11) aluminum base.

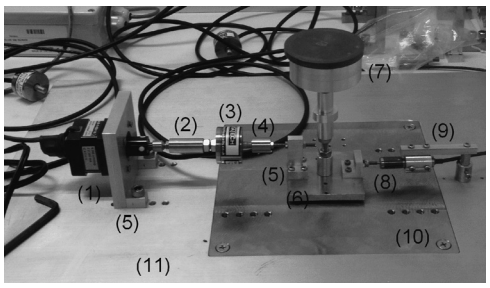

which correspond to the vertical forces applied at the contacts of the particles while the out-of-plan horizontal system and the vertical LVDT were not connected to the sled. A typical configuration during the calibration of the frictional force $F_{h,c}$ using dead loads is shown in **Fig. 14**. **Figure 15** shows the effect of the external vertical force on the friction produced by the bearing system of the sled, $F_{h,c}$. These results correspond to a sliding velocity equal to 600 μm/h. It is noted that the friction produced by the bearing system of the sled at zero external vertical force is because of the weight of the sled. In general, calibration tests in a range of sliding velocities between 0.15 and 4 mm/h showed that the effect of the sliding velocity on the frictional force $F_{h,c}$ is negligible. **Figure 16** shows the correction of the horizontal force measured by the load cell ($F_{h,\text{measured}}$) during an inter-particle shearing test. The general form of the relationship used to determine the corrected force, F_h, which is used for the calculations of the frictional force and the inter-particle coefficient of friction, is given by Eq 1.

$$F_h = F_{h,\text{measured}} - F_{h,b} - F_{h,c} \tag{1}$$

In Eq 1, $F_{h,\text{measured}}$ is the force recorded by the horizontal load cell during an inter-particle shearing test. $F_{h,b}$ is the frictional force produced by the bearing system of the sled and the linear bearings and is determined before the performance of a specific test by performing a calibration test following the same sliding track and the same sliding velocity as the inter-particle shearing test that follows, but the particles are not in contact during the calibration. Finally, $F_{h,c}$ is the frictional force produced by the bearing system of the sled because of the vertical load at the contact of the particles, and is determined through a series of calibration tests using dead loads.

Calculations

The forces developed at the contact of the particles during the inter-particle shearing tests and the equations, derived from

FIG. 15 The effect of the external vertical force on the friction of the bearing system of the sled at a sliding velocity of 600 μm/h (at zero external vertical load the friction is caused by the weight of the sled).

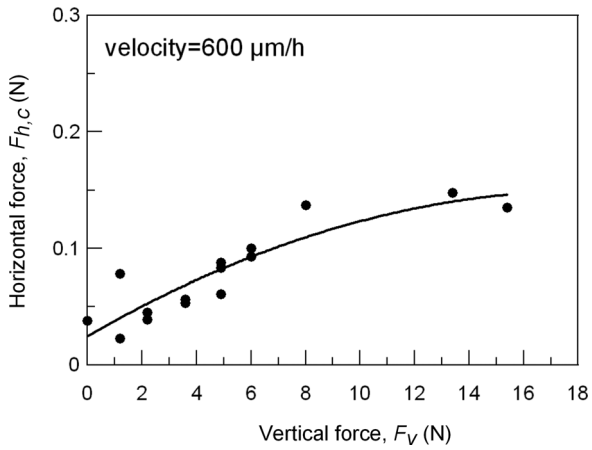

simple geometry, through which the inter-particle coefficient of friction is estimated, have been presented by Cavarretta et al. (2010, 2011). For the sake of completeness, we summarize in this paragraph these equations and illustrate qualitatively the response of the upper particle, which is stationary in the direction of shearing during the sliding of the lower one.

The frictional force, T, and the normal force, N, developed at the contact of the particles, are given as a function of the relative position of the two particles. This relative position is given as a function of the angle, α, between the contact plane and the horizontal as illustrated in **Fig. 17**. From simple geometry, the coefficient of friction is given as a function of the horizontal and vertical forces from Eq 2, and, thus, the estimation of the normal and frictional forces developed at the contact of the particles is given from Eqs 3 and 4.

$$\mu = \frac{F_h \times \cos\alpha - F_v \times \sin\alpha}{F_h \times \sin\alpha - F_v \times \cos\alpha} \tag{2}$$

FIG. 16 Correction of the horizontal force during an inter-particle shearing test.

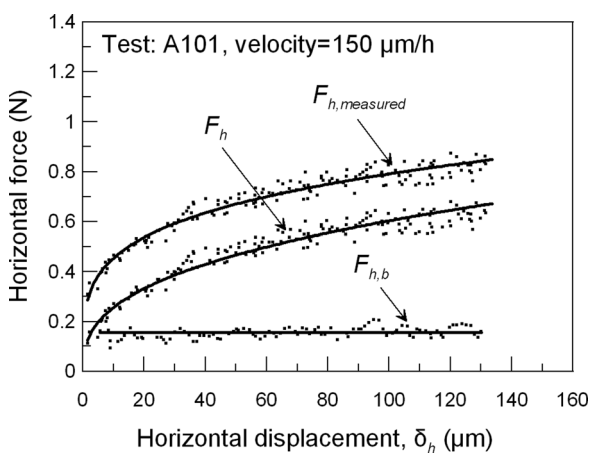

FIG. 17 Forces developed at the contact of the particles during a shearing test (the upper particle is stationary in the direction of sliding).

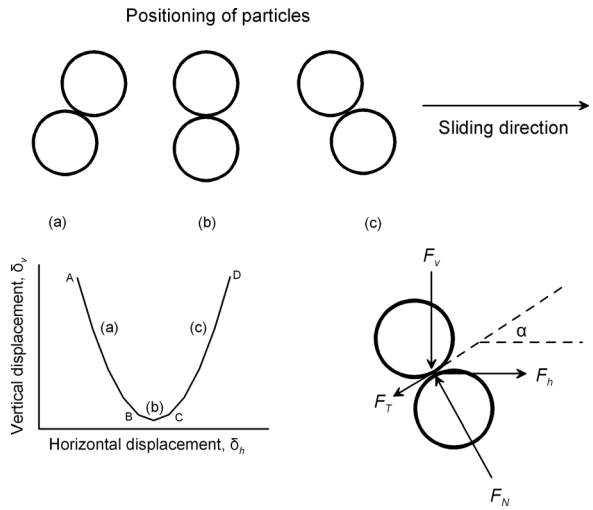

$$N = \frac{F_v \times \sin\alpha}{\cos\alpha - \mu \times \sin\alpha} \tag{3}$$

$$T = \mu \times N \tag{4}$$

The forces measured depend on the relative positions of the particles during the sliding. For example, as illustrated in **Fig. 17**, if the positions of the particles correspond to case (a), then the upper particle moves up, which is a "dilative" behavior, and the vertical displacement follows the path A → B (**Fig. 17**). At the point where the two particles are aligned at their apexes, which corresponds to case (b), the vertical displacement is constant, and, thereafter, (case (c)) the behavior is "contractive," and the vertical displacement follows the path C → D (**Fig. 17**).

It is noted that if the particles are not aligned close to their apexes in the out-of-plan direction, then the inter-particle coefficient of friction is overestimated using the procedure presented above (Cavarretta et al. 2011). Cavarretta et al. (2011) showed that if the angle, α_t, between the contact plane and the horizontal perpendicular to the sliding direction is less than 10°, then the measurements are consistent. To ensure that the angle α_t is less than 10°, the alignment of the particles, at the start and during the shearing tests, was checked using a digital micro-camera (**Fig. 6**), whereas, in the case of soil particles, only the ones with relatively convex and symmetrical shape were chosen for inter-particle shearing tests.

Proving Tests on Reference Particles

Twenty proving tests on reference chrome steel balls of 2.37 mm in diameter were carried out to assess the repeatability of the results and consistency with the literature data. Chrome steel balls were chosen because of their consistent surface chemistry and the minimum effect of the relative humidity on the inter-particle coefficient of friction (Cavarretta et al. 2011). These tests were performed on

oven-dried and air-equilibrated particles at room temperature and a relative humidity of about 22.5 °C to 24.5 °C and 93 % to 97 %, respectively. The tests were performed with a range of sliding velocities from 150 to 3600 μm/h and vertical confining forces between 1 and 10 N. Typical results are given in **Fig. 18**. In the figure, the inter-particle coefficient of friction is plotted against the horizontal displacement. The resultant inter-particle friction angle quoted corresponds to an average value along the shearing track.

In **Table 2**, the 20 experiments on reference particles are summarized. These data demonstrate high repeatability of the resultant coefficient of friction on the reference particles with values of the friction angle ranging between 4.5 ° and 8.5 °, approximately, with an average value of 6.4 ° and standard deviation equal to ±1.1 °. These data are consistent with the data on identical particles presented by Cavarretta et al. (2011), although the data from the new apparatus are significantly less scattered. The values of the friction angle, φ, presented in **Fig. 18** and **Table 2** and the inter-particle coefficient of friction, μ, presented in **Table 2** correspond to average values along the shearing track. Because of the steady state that is reached at relatively small displacements in most experiments, the inter-particle coefficient of friction is fairly constant along the shearing path in the majority of the tests. For example, in experiments A102 and B202 (**Fig. 18(*a*)** and **18(*b*)**), the inter-particle coefficient of friction slightly decreases at the start of shearing and reaches a fairly constant value at about 60 μm of horizontal displacement. In experiment C101A (**Fig. 18(*c*)**), it is noticed that the inter-particle coefficient of friction increases initially, reaching a constant value at about 40 μm of horizontal displacement. These differences are attributed partially to the effect of the initial alignment of the particles, which affects the response of the upper particle in the vertical direction.

In experiments A107A and A107B, the same particles were tested following the same shearing track. After the shearing test A107A, the particles were aligned at the same initial positions and a second inter-particle shearing test was performed following the same shearing track. The same procedure was followed for experiments C101A and C101B. These tests showed a small increase of the inter-particle coefficient of friction for the second test, which might be attributed to some damage occurring to the surfaces of the particles during the first test. The initial stiffness at the contact of the particles, which corresponds to the slope of the horizontal force–displacement diagram at small

FIG. 18 Typical inter-particle shearing test results on bearing balls of 2.37 mm in diameter (the friction angle values correspond to average values along the shearing track, $\varphi = \tan^{-1}(\mu) = \tan^{-1}(T/N)$).

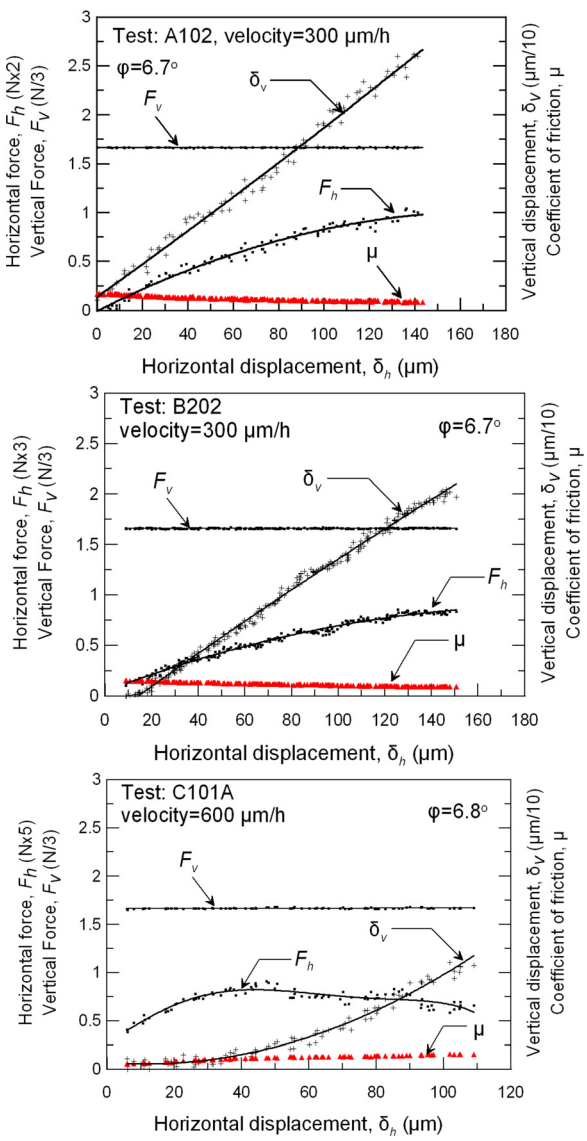

TABLE 2 Summary of the inter-particle shearing tests on chrome steel balls of 2.37 mm in diameter.

Code of Test	Sliding Velocity (μm/h)	F_v (N)	μ	φ	Frame
A101	150	4.89	0.097	5.5	1
A102	300	4.99	0.117	6.7	1
A103	300	4.99	0.097	5.5	1
A105	300	4.98	0.112	6.4	1
A106	600	4.99	0.119	6.8	1
A107A	600	0.98	0.078	4.5	1
A107B	600	0.98	0.096	5.5	1
A202	150	4.99	0.095	5.4	1
A203	600	4.99	0.118	6.7	1
A204	300	4.97	0.092	5.3	1
A205	900	4.97	0.115	6.6	1
A206	900	4.99	0.089	5.1	1
A207	300	5.00	0.122	7.0	1
A208	300	9.99	0.151	8.6	1
B201	150	4.98	0.134	7.6	1
B202	300	4.98	0.118	6.7	1
B203	1800	4.96	0.117	6.7	1
B204	3600	5.07	0.125	7.1	1
C101A	600	5.00	0.119	6.8	2
C101B	600	5.00	0.144	8.2	2

Note: F_v = vertical force, μ = inter-particle coefficient of friction, φ = inter-particle friction angle.

FIG. 19 Inter-particle shearing test results on Leighton Buzzard Sand quartz particles of 2.36–5.00 mm size (LBS05A and LBS12A: particles in dry state, LBS14: particle immersed in distilled water, $\varphi = \tan^{-1}(\mu) = \tan^{-1}(T/N)$).

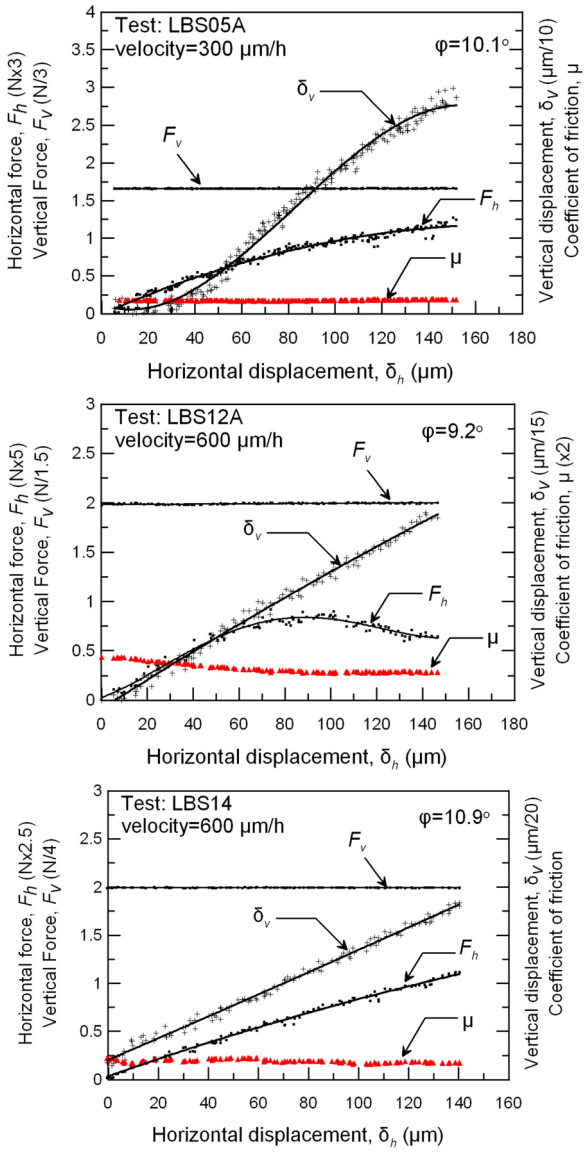

displacements, is lower than the initial stiffness of the apparatus in the direction of sliding. For example, for a vertical force equal to 5 N, the initial stiffness at the contact of the chrome steel balls ranges between 6 to 7 N/mm in most of the experiments.

Inter-Particle Shearing Tests on Typical Quartz Particles

Three tests were carried on Leighton Buzzard Sand quartz particles of 2.36–5.00 mm fraction at sliding velocities between 300 and 600 μm/h and vertical confining forces between 3 and 8 N. The results of the inter-particle shearing tests on the quartz particles are summarized in **Fig. 19**. In experiments LBS05A and LBS12A, the particles were tested in a dry state at room temperature and humidity of about 22.5 °C to 24.5 °C and 93 % to 97 %, respectively. In experiment LBS14, the particles were immersed in distilled water. Interferometer tests on particles from the same sample gave a surface roughness of 0.383 μm. This value corresponds to the root-mean-square deviation of the height of the surface (Sq). The particles tested in this study had relatively spherical shapes and were carefully selected after visual observation through an optical microscope.

As shown in **Fig. 19**, the inter-particle coefficient of friction is constant along the shearing track, in particular for horizontal displacements beyond 80 μm. The mean friction angle at the contact of the particles ranges narrowly between 9.2° and 10.9°. These values are very similar to the friction angle values on quartz minerals of relatively smooth surfaces presented by Horn and Deere (1962). For soil particles immersed in a viscous fluid, the true contact force may be less than that applied, so that the friction angle may perhaps be more correctly referred to as an "apparent friction angle." However, for tests on nominally dry soil particles and similar ones immersed in distilled water, Senetakis et al. (2013a) have noted no significant difference in friction angle, whereas Cavarretta et al. (2011) found a small anti-lubricating effect for water-immersed particles. For simplicity, the same symbols and expressions (i.e., φ, μ) are used here for both dry surfaces (tested at room humidity) and saturated surfaces.

Conclusions

A new, custom-built apparatus, capable of measuring the inter-particle coefficient of friction at the contacts of particles of sand to gravel size was presented in this paper. In the direction of sliding, the inter-particle shearing tests are performed through displacement control, while the vertical confinement at the contact of the particles is implemented through force control of the linear micro-stepping motors. For this purpose, new software was developed for the apparatus. The use of high-resolution linearly variable differential transformers, load cells of low capacity and high stiffness and resolution, as well as the use of high-quality amplifiers, signal conditioning, and data-logging systems allow very accurate measurements in the range of very small displacements of the order of tens to hundreds of microns with a minimum effect of the environmental and electrical noise.

Inter-particle shearing tests on reference particles composed of chrome steel balls and typical quartz particles of relatively convex shape demonstrated high repeatability of the results in terms of the average coefficient of friction along the shearing track and consistency with the data in the literature. The stiffness of the apparatus in the direction of sliding is sufficiently high to prevent stick-slip.

The new inter-particle shearing apparatus presented in this paper may provide useful input parameters to be used in computer codes that utilize the discrete element method.

Experimental data of high quality can be obtained for a variety of sliding velocities and confining forces, whereas the effects of variable parameters, such as the surface roughness and the parent material, can be investigated.

ACKNOWLEDGMENTS

The writers thank Dr. C. O'Sullivan from Imperial College for providing the chrome steel balls tested in this study, Dr. J. Wang and Ms. Rocchi from City University of Hong Kong for their constructive comments and suggestions, Dr. B. Baudet from Hong Kong University, and Ms. C. Todisco from City University of Hong Kong for the performance of interferometer tests on the quartz particles included in this study. The technicians from City University of Hong Kong, Mr. L.C. Mac and Mr. C.K. Lai, are also acknowledged for their technical support during the development of the new custom-built apparatus. This research work is supported by the Strategic Research Grant 7002667, "The development of a new soil particle loading apparatus" and the Start-Up Research Grant 9380056, "Experimental soil mechanics" funded by the City University of Hong Kong.

References

Barreto, D., 2009, "Numerical and Experimental Investigation into the Behaviour of Granular Materials under Generalised Stress States," Ph.D. thesis, Department of Civil Engineering, Imperial College of Science, Technology and Medicine, University of London, London.

Barreto, D. and O'Sullivan, C., 2012, "The Influence of Inter-Particle Friction and the Intermediate Stress Ratio on Soil Response under Generalised Stress Conditions," *Granular Matter*, Vol. 14, pp. 505–521.

Barton, R. R., 1972, "A Study of the Angle of Interparticle Friction of Sands with Respect to Its Influence on the Mass Strength," M.Sc. thesis, The Victoria University of Manchester, Manchester, U.K.

Burwell, J. T. and Rabinowicz, E., 1953, "The Nature of the Coefficient of Friction," *J. Appl. Phys.*, Vol. 24, No. 2, pp. 136–139.

Cavarretta, I., Coop, M., and O' Sullivan, C., 2010, "The Influence of Particle Characteristics on the Behavior of Coarse Grained Soils," *Geotechnique*, Vol. 60, No. 6, pp. 413–423.

Cavarretta, I., Rocchi, I., and Coop, M., 2011, "A New Interparticle Friction Apparatus for Granular Materials," *Can. Geotech. J.*, Vol. 48, No. 12, pp. 1829–1840.

Cundall, P. A., 1988, "Computer Simulations of Dense Sphere Assemblies," *Micromechanics of Granular Materials*, M. Satake and J. T. Jenkins (Eds.), Amsterdam, Elsevier, pp. 113–123.

Cundall, P. A. and Strack, O. D. L., 1979, "A Discrete Numerical Model for Granular Assemblies," *Geotechnique*, Vol. 29, pp. 49–65.

Horn, H. M. and Deere, D. U., 1962, "Frictional Characteristics of Minerals," *Geotechnique*, Vol. 12, No. 4, pp. 319–335.

Johnson, K. L., 1985, *Contact Mechanics*, Cambridge University Press, Cambridge, MA.

Kruyt, N. P. and Rothenburg, L., 2006, "Shear Strength, Dilatancy, Energy and Dissipation in Quasi-Static Deformation of Granular Materials," *J. Stat. Mech.*, Vol. 2006, p. P07021.

Kuhn, M. R., 1999, "Structured Deformation in Granular Materials," *Mech. Mater.*, Vol. 31, pp. 407–429.

Kuhn, M. R. and Mitchell, J. K., 1991, "New Perspectives on Soil Creep," *J. Geotech. Eng.*, Vol. 119, No. 3, pp. 507–524.

Kwok, C.-Y. and Bolton, M. D., 2010, "DEM Simulations of Thermally Activated Creep in Soils," *Geotechnique*, Vol. 60, No. 6, pp. 425–433.

Lu, M. and McDowell, G. R., 2010, "Discrete Element Modelling of Railway Ballast under Monotonic and Cyclic Triaxial Loading," *Geotechnique*, Vol. 60, No. 6, pp. 459–467.

Mindlin, R. D. and Deresiewicz, H., 1953, "Elastic Spheres in Contact under Varying Oblique Forces," *J. Appl. Phys.*, Vol. 63, pp. 327–343.

O'Sullivan, C., Cui, L., and O'Neill, S. C., 2008, "Discrete Element Analysis of the Response of Granular Materials during Cyclic Loading," *Soils Found.*, Vol. 48, No. 4, pp. 511–530.

Sazzad, Md. M. and Suzuki, K., 2011, "Effect of Interparticle Friction on the Cyclic Behavior of Granular Materials Using 2D DEM," *J. Geotech. Geoenviron. Eng.*, Vol. 137, No. 5, pp. 545–549.

Senetakis, K., Coop, M., and Todisco, M. C., 2013a, "The Inter-Particle Coefficient of Friction at the Contacts of Leighton Buzzard Sand Quartz Minerals," *Soils Found.*, Vol. 53, No. 5, pp. 746–755.

Senetakis, K., Coop, M., and Todisco, M. C., 2013b, "Tangential Load-Deflection Behaviour at the Contacts of Soil Particles," *Geotech. Lett.*, Vol. 3, pp. 59–66.

Shamy, U. El. and Denissen, C., 2011, "Microscale Energy Dissipation Mechanisms in Cyclically-Loaded Granular Soils," *J. Geotech. Geol. Eng.*, doi: 10.1007/s10706-011-9472-3.

Skinner, A. E., 1969, "A Note on the Influence of Interparticle Friction on Shearing Strength of a Random Assembly of Spherical Particles," *Geotechnique*, Vol. 19, pp. 150–157.

Thornton, C., 2000, "Numerical Simulations of Deviatoric Shear Deformation of Granular Media," *Geotechnique*, Vol. 50, No. 1, pp. 43–53.

Thornton, C. and Sun, G., 1993, "Axisymmetric Compression of 3D Polydisperse Systems of Spheres," *Powders and Grains*, Vol. 93, C. Thornton, Ed., Balkema, Rotterdam, The Netherlands, pp. 129–134.

Thornton, C. and Yin, K. K., 1991, "Impact of Elastic Spheres with and without Adhesion," *Powder Technol.*, Vol. 65, pp. 153–166.

Vu-Quoc, L. and Zhang, X., 1999. "An Accurate and Efficient Tangential Force-Displacement Model for Elastic Frictional Contact in Particle-Flow Simulations," *Mech. Mater.*, Vol. 31, pp. 235–269.

Wang, J. and Yan, H. B., 2012, "DEM Analysis of Energy Dissipation in Crushable Soils," *Soils Found.*, Vol. 52, No. 4, pp. 644–657.

Wang, J. and Yan, H. B., 2013, "On the Role of Particle Breakage in the Shear Failure Behavior of Granular Soils by DEM," *Int. J. Numer. Anal. Methods Geomech.*, Vol. 37, No. 8, pp. 832–854.

Yimsiri, S. and Soga, K., 2000, "Micromechanics-Based Stress–Strain Behaviour of Soils at Small Strains," *Geotechnique*, Vol. 50, pp. 559–571.

Yimsiri, S. and Soga, K., 2011, "Effects of Soil Fabric on Behaviors of Granular Soils: Microscopic Modeling," *Comput. Geotech.*, Vol. 38, pp. 861–874.